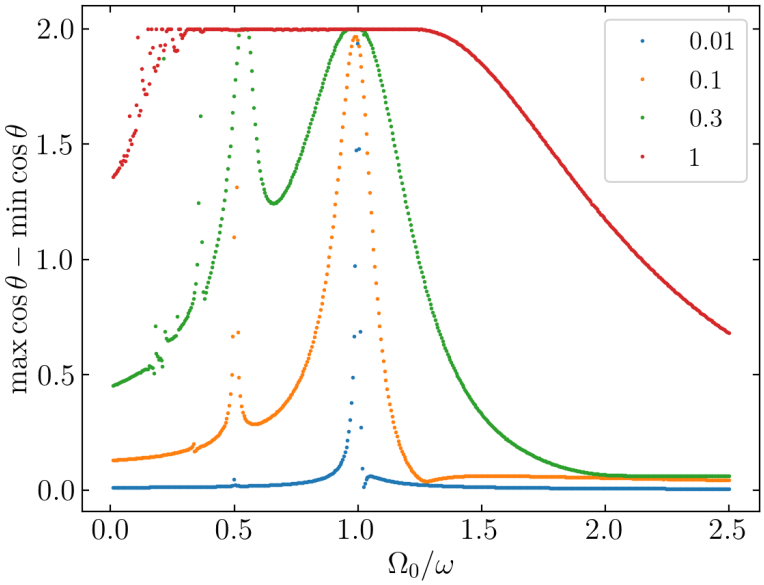

Figure 1: Plot of $\max\cos\theta_{\rm eff} - \min\cos\theta_{\rm eff}$ when solving Eq. (2). Legend denotes $\Omega_{\rm eff,1}/\Omega_{\rm eff}$. Orientation is $\arccos\left(\hat{\mathbf{z}}\cdot\hat{\mathbf{\Omega}}_{\rm eff,1}\right) = 60°$.

1 Recap

Recall EOM in corotating frame with $\hat{\mathbf{L}}$

$$\left(\frac{\mathrm{d}\hat{\mathbf{S}}}{\mathrm{d}t}\right)_{\rm rot} = \left(\Omega_{\rm SL}\hat{\mathbf{L}} - \dot{\Omega}\hat{\mathbf{z}}\right)\cdot\hat{\mathbf{S}} = \langle\Omega_{\rm SL}\hat{\mathbf{L}} - \dot{\Omega}\hat{\mathbf{z}}\rangle\times\hat{\mathbf{S}} + \left[\sum_{N=1}^{\infty}\mathbf{\Omega}_{\rm eff,N}\sin\left(2\pi N t/t_{\rm LK}\right)\right]\times\hat{\mathbf{S}}. \tag{1}$$

We have a good understanding of the non-adiabatic (fast-merger) regime. In the adiabatic regime, we expect good conservation of $\cos\theta_{\rm eff} = \hat{\mathbf{S}}\cdot\mathbf{\Omega}_{\rm eff}$, as the fast-varying terms should generally be able to be averaged over. We proposed the below toy model to understand the contribution of the leading-order $N = 1$ term, where we have rotated $\mathbf{\Omega}_{\rm eff} \propto \hat{\mathbf{z}}$:

$$\frac{1}{\Omega_{\rm eff}}\frac{\mathrm{d}\hat{\mathbf{S}}}{\mathrm{d}t} = \hat{\mathbf{z}}\times\hat{\mathbf{S}} + \sin(\omega t)\,\frac{\hat{\mathbf{\Omega}}_{\rm eff,1}}{\Omega_{\rm eff}}\times\hat{\mathbf{S}}. \tag{2}$$

Under the naïve expectation, where $\omega \gg \Omega_{\rm eff}, \Omega_{\rm eff,1}$, the second term should average away, and $\hat{\mathbf{S}}$ simply precesses around $\hat{\mathbf{z}}$, conserving $\theta_{\rm eff}$. Note that $\omega \Leftrightarrow 2\pi/P_{\rm LK}$ while $\Omega_{\rm eff} \simeq \dot{\Omega} \lesssim \omega$ is our regime of interest.

To estimate the deviation from exact conservation of $\theta_{\rm eff}$, we simulate $\mathrm{d}\hat{\mathbf{S}}/\mathrm{d}t$ for a long time and compute the total amplitude of oscillation of $\cos\theta_{\rm eff}$, and we found behavior as described in Fig. 1.

Per Dong's suggestion, the next step is to evaluate Eq. (2) with a real numerical LK spectrum, not restricting to the first harmonic.

2 This Week's Work

2.1 Change to $\theta_{\rm eff}$: Effect of I_0

Following the suggestion, I did not continue analytical work towards Eq. (2), but instead used a real LK spectrum. To be precise, for physical parameters from both the mild LK scenario (Paper I) and

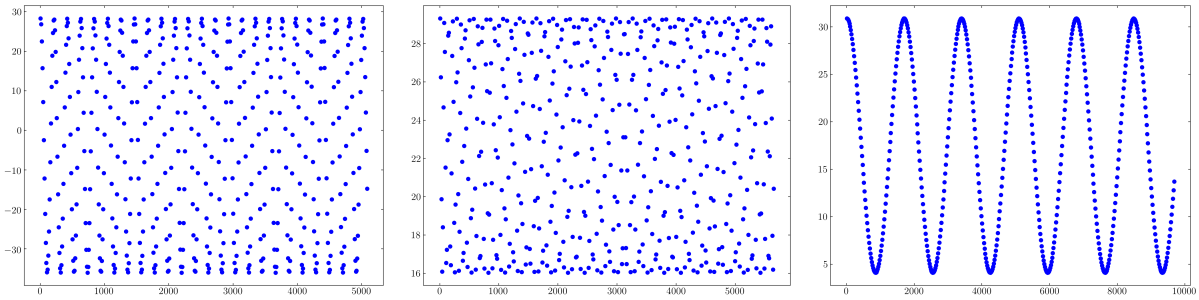

Figure 2: Plot of $\theta_{\rm eff}$ (y-axis) measured after each LK cycle using numerically integrated LK solution (x-axis is time in units of $t_{\rm LK}$). Physical parameters are from Paper I, $e_0 = 0.003$ and $I_0 = 117.543^\circ$, 120°, and 125.15° respectively.

the distance LK scenario (Paper II), I solved the GW-free (but including de Sitter precession) LK oscillation equations and obtained $\dot{\Omega}$, $\Omega_{\rm SL}$, and $\hat{\mathbf{L}}$ over a single LK period. I then evolve $\hat{\mathbf{S}}$ using the first EOM in Eq. (1) over 500 LK periods, using the numerical LK solution over each period. I then measure $\theta_{\rm eff}$ at the end of every LK period, and plot $\theta_{\rm eff,max} - \theta_{\rm eff,min}$[1]. I start at a variety of initial I_0, but use a uniform initial eccentricity $e_0 = 0.003$ (slightly larger than the values used in Paper I, Paper II, to account for some small initial GW dissipation). I choose the initial $\hat{\mathbf{S}}$ to lie along $\hat{\mathbf{L}}$ for simplicity; I explore the effect of varying initial conditions later. Three sample trajectories for the Paper I scenario have similar I (117.543°, 120°, 125.15°) but significantly different amplitudes of $\theta_{\rm eff}$ excursions are shown in Fig. 2. As can be seen, the two large-amplitude oscillations have notably different characters, owing to their belonging to two different types of resonances; we explain this later.

I tried this for both Paper I and Paper II; Paper I's scenario is useful to calibrate against because we know what range of I_0 experience $\theta_{\rm eff}$ excursions, even though Paper II's parameters are more physically relevant. Both are presented in Fig. 3. It is evident that Paper II's scenario conserves $\theta_{\rm eff}$ quite well. Comparison to the results of Paper I shows that substantial $\theta_{\rm eff}$ excitation is indeed possible, and occurs at particular values of I_0 given a particular e_0. Including GW dissipation, which changes both I_0 and e_0 (initial inclinations/eccentricities at the start of each LK cycle), this implies a large range of initial $(I, e = 0.001)$ can experience $\theta_{\rm eff}$ excitation over the course of GW radiation (the bounds are believably consistent).

Above, we said we fixed $\hat{\mathbf{S}}_{\rm i} = \hat{\mathbf{L}}_0$. I also explored the variation of $\max\theta_{\rm eff} - \min\theta_{\rm eff}$ as a function of (θ, ϕ) (in coordinates where $\hat{\mathbf{L}}_{\rm out} \propto \hat{\mathbf{z}}$). I am currently regenerating these plots for particularly interesting I_0, but one for the Paper II regime and $I_0 = 125^\circ$ is given in Fig. 4.

2.2 Contributing Factors to Resonance

Based on the toy model from the previous week (Fig. 1), we know the two primary contributing factors to the amplitude of the $\theta_{\rm eff}$ oscillations are: (i) the strength of the $N = 1$ term ($\sim \Omega_{\rm eff,1}/\Omega_{\rm eff}$ up to a projection factor), which sets the width of the resonance(s); and (ii) the ratio $\langle\Omega_{\rm eff}\rangle P_{\rm LK}/(2\pi)$, which sets whether we are near a resonance. (iii) A third one is the alignment between the $N = 0$ and $N = 1$ component of $\mathbf{\Omega}_{\rm eff}$; this proves not particularly useful as all Fourier components are generally quite well aligned (the vectors they approximate are close to delta functions at the eccentricity maxima).

We make plots of all three of these in Fig. 5.

[1] This amplitude is of interest since it provides an upper bound on $\theta_{\rm eff}$ excitations when hitting a resonance; the actual excitation versus this upper bound will be considered another week, but must depend on the adiabaticity of resonance crossing.

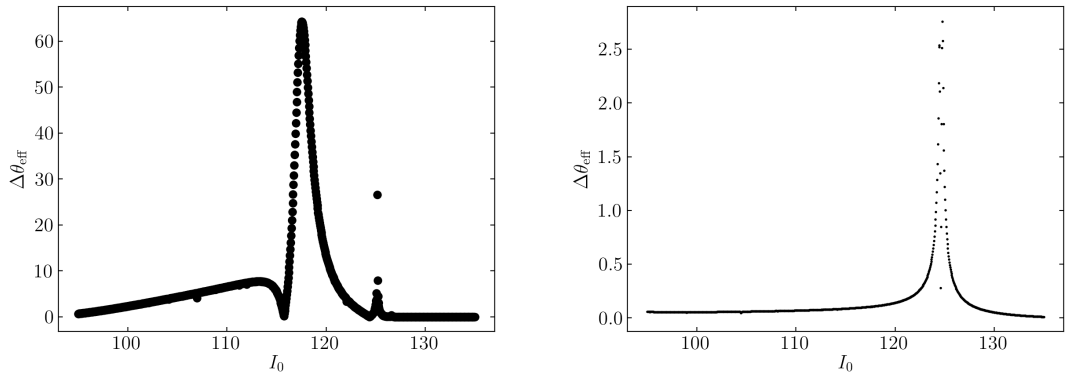

Figure 3: $\theta_{\rm eff,max} - \theta_{\rm eff,min}$ (in degrees) using numerical LK solutions to evolve an initial spin $\hat{\mathbf{S}} = \hat{\mathbf{L}}$ by 500 LK cycles, for $e_0 = 0.003$ in the Paper I and Paper II regimes respectively. Inclinations are sampled $I_0 \in [95°, 135°]$.

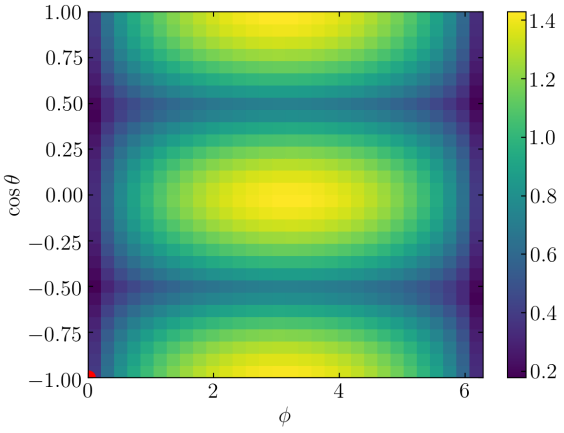

Figure 4: $\theta_{\rm eff}$ for various possible $\hat{\mathbf{S}}$ initial conditions. The angular variation is relatively smooth.

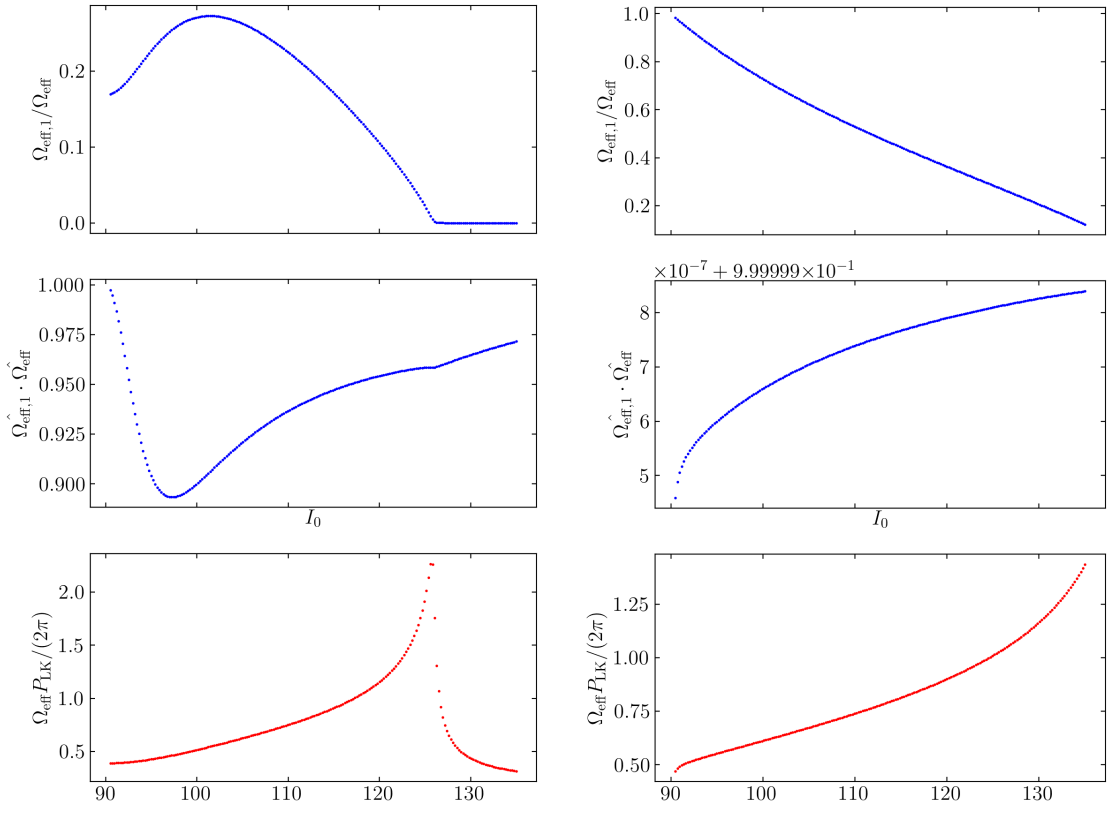

Figure 5: Plot of the ratio of $N = 1$ to $N = 0$ (in magnitude).

This paints an encouraging picture. If, for each I_0, we take the ratio in the third panel, and look at Fig. 1, this seems to coarsely predict the correct behavior in Fig. 3. Further work is needed to confirm this.

2.3 Qualitative Picture So Far

We have restricted $e_0 = 0.003$ in Section 2.1, so we will focus on this case, and we have restricted $I_0 \in [95^\circ, 135^\circ]$.

Based on Fig. 5, in the Paper I scenario, we expect a $\Omega_0/\omega = 1$ resonance at around 117° and a $\Omega_0/\omega = 0.5$ resoonance at around 127°. In the Paper II scenario, the $\Delta\Omega = \pi$ resonance is missed by our I_0 range (I will fix), and instead deviations from adiabaticity are generated by the $\Delta\Omega = 2\pi$ resonance, which is very weak since it occurs for $I \gtrsim 130^\circ$ where the $N = 1$ Fourier coefficient is very weak (Fig. 5) and LK oscillations disappear. Both of these match quite well with Fig. 3.

The necessary/possible next objectives are:

- Examine $I_0 \approx 92.5^\circ$ for the Paper II regime, where there is likely another resonance, much stronger than the effect observed in Fig. 3.
- Understand how the resonance sweeps through trajectories under GW decay (increase of e_0 and decrease of I_0 from initial conditions)
- Analytical understanding of $\Delta\Omega = \pi$ resonance.